

Solving the angular momentum problem in the cold feedback mechanism of cooling flows

Fabio Pizzolato ^{*}

INAF–Osservatorio Astronomico di Brera, Via Brera n.28, 20121 Milano (Italy)

Noam Soker [†]

Physics Department, Technion, Haifa 32000 (Israel)

24th October 2018

ABSTRACT

We show that cold clumps in the intra-cluster medium (ICM) efficiently lose their angular momentum as they fall in, such that they can rapidly feed the central AGN and maintain a heating feedback process. Such cold clumps are predicted by the cold feedback model, a model for maintaining the ICM in cooling flows hot by a feedback process. The clumps very effectively lose their angular momentum in two channels: the drag force exerted by the ICM and the random collisions between clumps when they are close to the central black hole. We conclude that the angular momentum cannot prevent the accretion of the cold clumps, and the cold feedback mechanism is a viable model for a feedback mechanism in cooling flows. Cold feedback does not suffer from the severe problems of models that are based on the Bondi accretion.

Key words: galaxies: clusters: intracluster medium galaxies: clusters: cooling flows galaxies: clusters: general galaxies: clusters: individual: Virgo

1 INTRODUCTION

For more than a decade now it is clear that the intra-cluster medium (ICM) in cooling flow (CF) clusters of galaxies and CF galaxies must be heated, and the heating process should be stabilized by a feedback mechanism (see reviews by [Peterson & Fabian 2006](#) and

^{*} E-mail: fabio.pizzolato@brera.inaf.it

[†] E-mail: soker@physics.technion.ac.il

McNamara & Nulsen 2007). However, in many cases the heating cannot completely offset cooling (e.g., Wise et al. 2004; McNamara et al. 2004; Clarke et al. 2004; Hicks & Mushotzky 2005; Bregman et al. 2006; Salomé et al. 2008; Wilman et al. 2009) and some gas cools to low temperatures and flows inward (e.g., Peterson & Fabian 2006). The mass inflow rate is much below the one that would occur without heating, and the flow is termed a moderate cooling flow (Soker et al. 2001; Soker & David 2003; Soker 2004).

Two basic modes have been proposed to feed the super massive black hole (SMBH) at the heart of the active galactic nucleus (AGN) in CF clusters (e.g., Combes 2008). They can be termed the hot and the cold feedback mechanisms. In the hot-feedback mode the hot gas from the vicinity of the SMBH is accreted, such as in the Bondi accretion process (e.g., Omma & Binney 2004; Allen et al. 2006; Russell et al. 2010). More sophisticated schemes that use direct calculations of the inflow of the hot gas, but are basically similar to the Bondi accretion process, also exist (e.g., Ciotti et al. 2009, 2010). However, the Bondi accretion process suffers from two severe problems (Soker 2006; Soker et al. 2009), to the point that it fails. First, there is no time for the feedback to work. The accretion of gas from the very inner region does not have time to respond to gas cooling in the outer regions ($r \gtrsim 10$ kpc). Second, although in galaxies the accretion rate can in principle account for the AGN power (Allen et al. 2006; Ciotti et al. 2009, 2010), in CF clusters the Bondi accretion rate is much too low (Rafferty et al. 2006). In a recent paper it was argued that the Bondi accretion process fails to maintain feedback in the process of galaxy formation as well (Soker 2009).

In the cold feedback model (Pizzolato & Soker 2005; Soker 2006; Pizzolato 2007) the mass accreted by the central black hole originates in non-linear over-dense blobs of gas residing in an extended region of $r \sim 5 - 30$ kpc; these blobs are originally hot, but then cool faster than their environment and sink toward the centre (see also Revaz et al. 2008). The mass accretion rate by the central black hole is determined by the cooling time of the ICM, the entropy profile, and the presence of inhomogeneities (Soker 2006). In the cold feedback model if gas cools at large distances, so do the overdense blobs. In a relatively short time they feed the SMBH, and the ICM is heated on a time scale shorter than its cooling time scale. This overcomes the main problem of models based on the Bondi accretion process (Soker 2009). Wilman et al. (2009) suggest that the behaviour and properties of the cold clumps they observe in the cluster A 1664 support the cold feedback mechanism. In general, the presence of large quantities of cold ($T \lesssim 10^4$ K) gas in CF clusters (e.g., Edge et al.

2002; Edwards et al. 2007) suggests that the non-linear perturbations that are required to form the dense clumps do exist in CF clusters.

The main arguments against the cold feedback mechanism was that the cold clumps supposed to feed the SMBH have too much angular momentum, and they cannot fall directly to the SMBH: for this reason, their accretion rate will be too slow and the response time too long (e.g., Russell et al. 2010).

In this paper we show that dense clumps lose their angular momentum rapidly enough, such that there is no angular momentum problem in the cold feedback mechanism. The equations are presented in Sections 2 and 3, and the cluster properties used for the calculations are given in Section 4. In Section 5 we present the solution for falling clumps, both without (Sec. 5.1) and with (Sec 5.2) angular momentum. In Section 6 the loss of angular momentum via collision is estimated. Our main conclusions are in Section 7.

2 EQUATIONS OF MOTION

Following Pizzolato & Soker (2005) (also Paper I), we write the set of equations governing the motion of a cold clump in the ICM. In Paper I we adopted the following equations for the motion of a clump:

$$\frac{d\mathbf{x}}{dt} = \mathbf{v} \quad (1a)$$

$$\rho' V \frac{d\mathbf{v}}{dt} = -\frac{C_D}{2} S \rho |\mathbf{v}| \mathbf{v} + \mathbf{g} (\rho' - \rho) V, \quad (1b)$$

where the primed quantities refer to the clump. The first equation relates the position \mathbf{x} of the clump with its velocity \mathbf{v} ; the second is Newton's second law for the clump's motion: V is the volume of the clump, and $\rho' V$ its mass. The first term on the right-hand side is the drag force, where $C_D \simeq 0.75$ (Kaiser 2003) is the drag coefficient and S the clump's cross section. The second term is the gravitational force, corrected for the buoyancy.

These equations must be completed with the evolution of the density of the clump, which we give in a slightly different form than in Paper I. Let $s(\mathbf{x}, t)$ and $s'(\mathbf{x}, t)$ be the specific entropies of the ICM and of a clump at the time t and position \mathbf{x} . We assume that the clump is always in pressure equilibrium with the ICM: $P = P'$. For this reason the specific entropy s' of an overdense clump is lower than the ICM specific entropy. Let

$$\Delta s(\mathbf{x}, t) = s'(\mathbf{x}, t) - s(\mathbf{x}, t) \quad (2)$$

be the entropy difference between the clump and the ambient ICM at the time t . We now

consider the evolution of Δs at a later instant $t + dt$. On account of the radiative losses both the ICM and the clump have cooled. The entropy profile of the ambient gas at $t + dt$ is

$$s(\mathbf{x}, t + dt) - s(\mathbf{x}, t) = -\frac{n_e n_H \Lambda(T)}{n T} dt, \quad (3)$$

where $\Lambda(T)$ is the cooling function, n_e , n_H and n being the electron, proton and total density of the ICM ¹. At the same instant $t + dt$ the entropy content of the clump has changed as well due to the radiative losses:

$$s'(\mathbf{x} + d\mathbf{x}, t + dt) - s'(\mathbf{x}, t) = -\frac{n'_e n'_H \Lambda(T')}{n' T'} dt, \quad (4)$$

The position is now evaluated at $\mathbf{x} + d\mathbf{x}$ because the clump is denser than the environment, so it has sunk a little, moving from \mathbf{x} to $\mathbf{x} + d\mathbf{x}$. The entropy contrast with the ambient gas at the new position of the clump is

$$\Delta s(\mathbf{x} + d\mathbf{x}, t + dt) = s'(\mathbf{x} + d\mathbf{x}, t + dt) - s(\mathbf{x} + d\mathbf{x}, t + dt). \quad (5)$$

Subtracting equations (5) and (2) taking into account equations (3) and (4) we find the variation of the entropy contrast:

$$d\Delta s = \Delta s(\mathbf{x} + d\mathbf{x}, t + dt) - \Delta s(\mathbf{x}, t) = -\frac{n'_e n'_H \Lambda(T')}{n' T'} dt + \frac{n_e n_H \Lambda(T)}{n T} dt - \nabla s \cdot d\mathbf{x} \quad (6)$$

The entropy contrast Δs may be expressed in term of the density contrast

$$\delta = (n' - n)/n \quad (7)$$

under the isobaric assumption $P \equiv P'$ between the clump and the ICM:

$$\Delta s = \frac{3}{2} k_B \ln \left(\frac{P'}{n'^{5/3}} \right) - \frac{3}{2} k_B \ln \left(\frac{P}{n^{5/3}} \right) = -\frac{5}{2} k_B \ln(1 + \delta); \quad (8)$$

notice that if $\delta = 0$ the entropy contrast vanishes. Equation (6) may then be written

$$\frac{5}{2} \frac{1}{1 + \delta} \frac{d\delta}{dt} = \frac{3}{2} \mathbf{v} \cdot \nabla \ln K + \frac{n'_e n'_H \Lambda(T') - n_e n_H \Lambda(T)}{P}, \quad (9)$$

where we have introduced the pressure $P' = P = nk_B T$ and the entropy index $K = T/n_e^{2/3}$, connected to the specific entropy s through the relation

$$s = \frac{3}{2} k_B \ln K. \quad (10)$$

The temperature of the clump is related to that of the ambient gas through the isobaric condition

$$T' = T/(1 + \delta). \quad (11)$$

¹ In the present analysis we neglect the “background” flow due to the cooling of the ICM. The effect of this term was addressed by [Loewenstein \(1989\)](#). Its inclusion would require some modelling of the background flow. The impact on the results is weak, and does not justify the amount of required work.

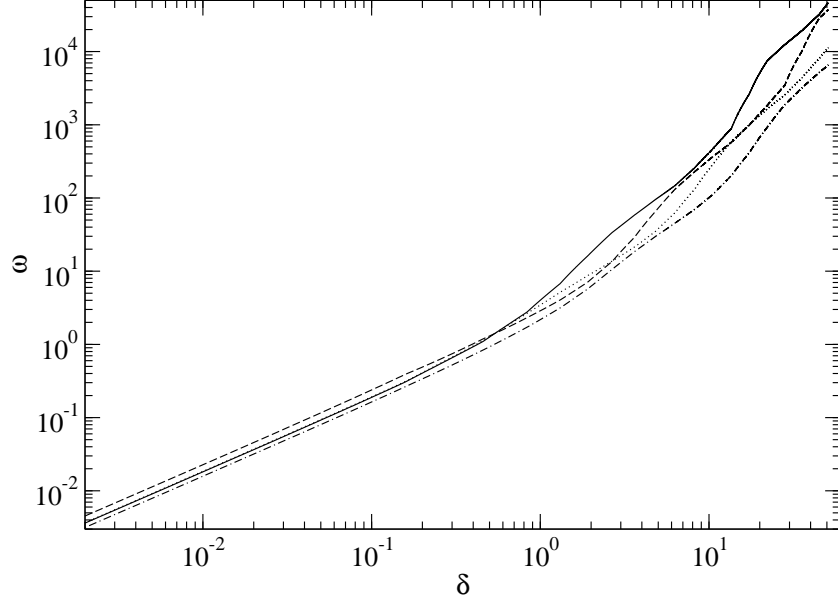


Figure 1. Plot of the function $\omega(\delta, T)$ defined by Equation (13). δ is the density contrast (eq. 7), while ω is a function that enters the equation describing the relative evolution of the clump and the ICM; the larger ω is, the faster is the evolution of the clumps due to radiative cooling. Terms due to buoyancy and to radiative cooling appear in ω . The cooling function used to draw this plot has metal abundance $Z = 0.3$ (Anders & Grevesse 1989 solar units). The curves refer to different temperatures: $T = 0.5$ keV (solid line), $T = 1.0$ keV (dashed line), $T = 2.0$ keV (dotted line) and $T = 4.0$ keV (dash-dotted line).

With the aid of this constraint we may rewrite Equation (9)

$$\frac{5}{2} \frac{1}{1 + \delta} \frac{d\delta}{dt} = \frac{3}{2} \mathbf{v} \cdot \nabla \ln K + \frac{\mu_H n_e \Lambda(T)}{k_B T} \omega(\delta, T), \quad (12)$$

where $\mu_H = n_H/n \simeq 0.44$. The function

$$\omega(\delta, T) = \frac{(1 + \delta)^2}{\Lambda(T)} \Lambda \left(\frac{T}{1 + \delta} \right) - 1, \quad (13)$$

is plotted in Fig. 1 for several values of T . Note that for small values of δ the profiles are very similar to each other, since $\delta \ll 1$ implies $\omega \simeq (2 - d \ln \Lambda / d \ln T) \delta$ for any T .

Since relaxed clusters are convectively stable, the entropy gradient is positive, and since \mathbf{v} is directed inwards, the first term on the right-hand side of Equation (12) is negative, and tends to stabilise the clump, i.e. to keep its density contrast small. This term is responsible for the stability of clumps with small density contrasts. The second term describes the clump's instability to its own radiative cooling with respect to the ICM. It has the sign of ω , which is usually positive for $\delta > 0$, thus giving a positive contribution to $\dot{\delta}$. As discussed in more detail in Appendix A, for small δ this term is responsible for an overstability of the clump, as already found and discussed by Balbus & Soker (1989).

As pointed out by Burkert & Lin (2000), when the cooling time of the clump falls below the sound crossing time, the pressure equilibrium does not hold any longer, and the clump

evolves isochorically. For consistency, we shall have to check *a posteriori* that the clump does not enter this regime during its evolution.

Equation (12) is the same equation for the evolution of the density contrast δ adopted in Paper I if the term with the ICM cooling is dropped. The new equation expresses more transparently than in Paper I the role of the ambient entropy gradient in the clumps' accretion (Soker 2006). The dynamical status of the overdensity (the right-hand side of Equation 12) depends on the properties of the clump only through its overdensity: the remaining controlling parameters only depend on the ICM temperature, density and entropy distributions. At this stage, we are neglecting the ICM heating due to the AGN activity, and we only consider its radiative cooling. The ICM cooling term makes the clumps slightly more stable than considered in Paper I, where even a clump of zero overdensity gave a positive contribution to $\dot{\delta}$.

3 THE ANGULAR MOMENTUM

As in Paper I, we follow the evolution of a clump, but the purpose of this study is to address more fully the issue of the clump's angular momentum. If the clump is not able to lose effectively its angular momentum, it cannot be accreted by the AGN rapidly enough, and the feedback cannot work.

We estimate the time scale taken by the drag force to dissipate the angular momentum of the clump. Taking the vector product of \mathbf{x} by Equation (1b) we get

$$\frac{d\mathbf{l}}{dt} = -\frac{3}{8} \frac{C_D |\mathbf{v}|}{a(1+\delta)} \mathbf{l} \quad (14)$$

where a is the radius of the clump (assumed spherical) and $\mathbf{l} = \mathbf{x} \times \mathbf{v}$ is the specific angular momentum. Note that since $\mathbf{l} \times \dot{\mathbf{l}} = 0$ the orbit of a clump is planar. The characteristic time of angular momentum loss is

$$\tau_l = \mathbf{l} / \dot{\mathbf{l}} = \frac{8}{3} \frac{a(1+\delta)}{C_D |\mathbf{v}|} \simeq 1.2 \times 10^7 \text{ yr} \left(\frac{a}{100 \text{ pc}} \right) \left(\frac{1+\delta}{10} \right) \left(\frac{\sigma}{300 \text{ km s}^{-1}} \right)^{-1}, \quad (15)$$

where we have equalled $|\mathbf{v}|$ to a typical velocity dispersion σ . This time is to be compared to the time of a Keplerian revolution to give

$$\tau_l / \tau_K \simeq (1+\delta)a/r \quad (16)$$

For $\delta \simeq 10$, $a \simeq 100 \text{ pc}$ and $r \simeq 10 \text{ kpc}$ this ratio is $\tau_l / \tau_K \simeq 10^{-1} \ll 1$. Therefore a clump of moderate overdensity is expected to quickly lose its angular momentum and fall straight on the AGN. An exception to this occurs when the cooling time of the clump is much less than

τ_l . In this case, the clump becomes very dense ($\delta \gg 1$) before losing its angular momentum. For $\delta \gg 1$ the drag force is small, and the clump may orbit around the centre losing but slowly its angular momentum. This approximate derivation must be complemented by a more accurate numerical calculation, presented in Section 5.

Since the orbit of a clump is planar, the differential equations for its (isobaric) evolution may be written in two-dimensional polar coordinates (r, ϕ)

$$\frac{dr}{dt} = u \quad (17a)$$

$$\frac{d\phi}{dt} = l/r^2 \quad (17b)$$

$$\frac{du}{dt} = \frac{l^2}{r^3} - \frac{3}{8} C_D \frac{|\mathbf{v}|}{a(1+\delta)} u - g \frac{\delta}{1+\delta} \quad (17c)$$

$$\frac{dl}{dt} = -\frac{3}{8} C_D \frac{|\mathbf{v}|}{a(1+\delta)} l \quad (17d)$$

$$\frac{d\delta}{dt} = (1+\delta) \left[\frac{3}{5} \frac{u}{r} \frac{d \ln K}{d \ln r} + \frac{2}{5} \frac{\mu_H n_e \Lambda(T)}{k_B T} \omega(\delta, T) \right], \quad (17e)$$

where u is the radial velocity, l the modulus of the angular momentum, $g = |\mathbf{g}|$ is the modulus of the gravitational acceleration, and

$$|\mathbf{v}| = (u^2 + l^2/r^2)^{1/2} \quad (18)$$

is the modulus of the velocity.

The last equation we need governs the evolution of the clumps' size a . There are different possible choices here: the most straightforward one implements the conservation of the clump's mass

$$a = a_0 \left[\frac{1+\delta_0}{1+\delta} \frac{n_e(r_0)}{n_e(r)} \right]^{1/3}, \quad (19)$$

where r_0 is the initial radial distance of the clump from the centre, a_0 and δ_0 are the initial clump's radius and overdensity, respectively. On the other hand, as a clump becomes dense and moves through the ICM, it may lose its spherical shape, or even break up into several smaller clumps. The fragmentation (or mass loss) is clearly inconsistent with the conservation law (19), so we shall have to implement the description of this phenomenon at some level. The process of fragmentation is quite complex and beyond the scope of the present paper, so we take a phenomenological stand, and assume that at each radial distance from the centre r the mass of the clump m is reduced with respect to its initial value m_0 according to the prescription

$$m = m_0 (r/r_0)^k, \quad (20)$$

where the mass loss index $k \geq 0$ is a constant. This prescription is equivalent to

$$a = a_0 \left[\left(\frac{r}{r_0} \right)^k \frac{1 + \delta_0}{1 + \delta} \frac{n_e(r_0)}{n_e(r)} \right]^{1/3}, \quad (21)$$

which reduces to the mass conservation (19) if $k = 0$. Note that the decrease of a implied by Equation (21) has the same effect to increase the cross section to volume ratio, which mimics the clump's loss of spherical symmetry, with the major axis aligned with the direction of motion.

Note that Equation (20) properly describes the effects of loss of shape and/or break up if the clump does not oscillate across the ICM, since in this case $m(t)$ would not be a monotonic function of time.

In Section 5 we shall solve numerically the system of equations (17) separately for the prescriptions (19) and (21). In Appendix A we present an analysis of the equilibrium solutions of Equations (17) (with the conservation condition 19), and also provide an approximate stability criterion for the evolution of a clump (see also Balbus & Soker 1989; Tribble 1991).

4 CHOICE OF THE CLUSTER PROFILES

As in Paper I, we focus on a specific cluster, i.e. Virgo. We adopt the entropy, temperature and electron density profiles derived by Cavagnolo et al. (2009)². We fit the 3D electron density with a double beta model

$$n_e = \frac{n_1}{[1 + (r/r_1)^2]^{\beta_1}} + \frac{n_2}{[1 + (r/r_2)^2]^{\beta_2}}. \quad (22)$$

The 3D entropy index profiles are modelled by Cavagnolo et al. (2009) with the simple formula

$$K = K_0 + K_1 \left(\frac{r}{100 \text{ kpc}} \right)^\alpha. \quad (23)$$

These entropy profiles have been deduced from non-deprojected (2D) temperatures: according to Cavagnolo et al. (2009) this does not affect the determination of the 3D entropy profiles appreciably. The temperature profiles provided by Cavagnolo et al. (2009) are 2D. Since Virgo is almost isothermal (see e.g. Ghizzardi et al. 2004), we do not expect that the use of 2D instead of 3D profiles will severely affects our results. We then use the 2D

² Their data (for a sample of 239 clusters observed with *Chandra*) may be found at <http://www.pa.msu.edu/astro/MC2/accept/>.

2D temperature					
T_0 (keV)	T_1 (keV)	r_t (kpc)	γ		
1.893	3.022	29.36	1.543		
3D electron density					
n_1 (10^{-2} cm^{-3})	r_1 (kpc)	β_1	n_2 (10^{-2} cm^{-3})	r_2 (kpc)	β_2
1.320	8.762	0.24	15.08	1.896	0.819
3D entropy index					
K_0 (keV cm ²)	K_1 (keV cm ²)	α			
3.53	146.6	0.8			

Table 1. Best fitting parameters for the (projected) temperature, and 3D electronic density and entropy index for Virgo. More details in the text.

temperature profile as an estimate of the real 3D profile, and we fit it with the expression

$$T = \frac{T_0 + T_1(r/r_t)^\gamma}{1 + (r/r_t)^\gamma}, \quad (24)$$

already used by [Vikhlinin et al. \(2006\)](#) to model the temperature of galaxy clusters in their cool cores. The profiles (22) and (24) are used to determine the hydrostatic gravitational acceleration

$$g = \frac{G M(< r)}{r^2} = \frac{k_B T}{\mu m_u r} \left(\frac{d \ln n_e}{d \ln r} + \frac{d \ln T}{d \ln r} \right), \quad (25)$$

where $M(< r)$ is the gravitating mass within the radius r , m_u is the atomic mass unit and $\mu \simeq 0.6$ is the mean molecular weight. Table 1 presents the best-fitting values of the fit parameters for the electron density, temperature and entropy profiles. The profiles for Virgo of T , n_e , K and $M(< r)$ are plotted in Fig. 2, compared to the original data from [Cavagnolo et al. \(2009\)](#).

Throughout this paper we assume that the metal abundance is 0.3 times the solar value ([Cavagnolo et al. 2009](#)), with the heavy element ratios taken from [Anders & Grevesse \(1989\)](#).

5 NUMERICAL CALCULATIONS

In this section we solve numerically equations (17) with the temperature, entropy and density profiles presented in Section 4. We adopt the embedded Runge-Kutta Prince-Dormand (8,9) method (e.g., [Press et al. 2007](#)) implemented in the GNU scientific library ³. The cooling function Λ has been calculated with the XSPEC package for the APEC atomic tables.

In the next two subsections we present the evolution of the clumps with and without angular momentum.

³ http://www.gnu.org/software/gsl/manual/html_node/Ordinary-Differential-Equations.html.

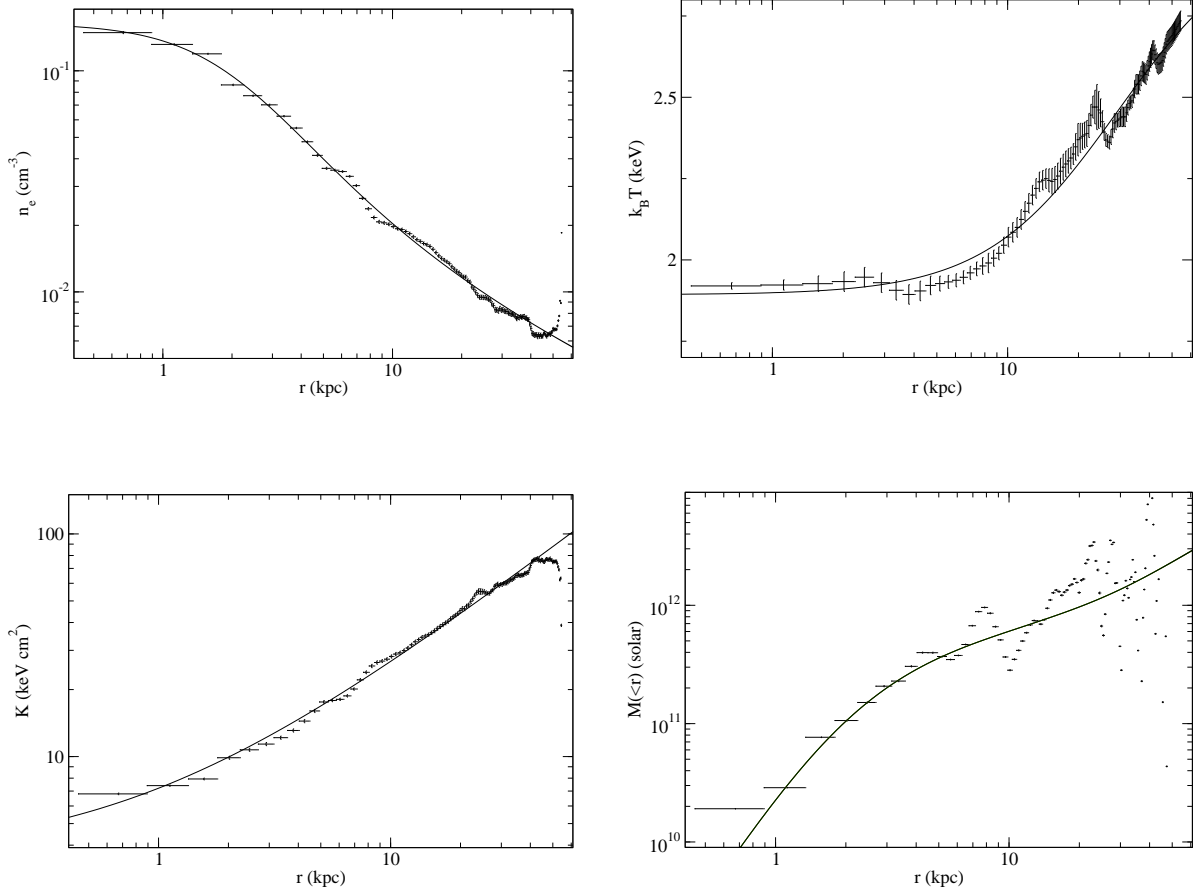


Figure 2. Best fitting profiles for the electron density (top left), temperature (top right), entropy index (bottom left) and gravitating mass (bottom right) profiles adopted for Virgo, superposed to the data by [Cavagnolo et al. \(2009\)](#).

5.1 Zero Angular Momentum

We follow the evolution of a clump of initial radius $a_0 = 100$ pc released from rest at a distance $r_0 = 20$ kpc from the cluster's centre. We distinguish the case where the clump conserves its mass during the inflow, from the case where the clump undergoes fragmentation.

5.1.1 Constant Mass Clumps

The size of a constant mass clump is given, instant by instant, by the conservation condition (19). We may distinguish three regimes for the accretion of such a clump: stable, relatively unstable and absolutely unstable.

These regimes are exemplified in Fig. 3, showing the evolution of a clump for different initial values of the overdensity: $\delta_0 = 1.4$ (solid line), $\delta_0 = 2.0$ (dashed line) and $\delta_0 = 3.0$ (dotted line). The top left panel of Fig. 3 shows the evolution of the overdensity defined

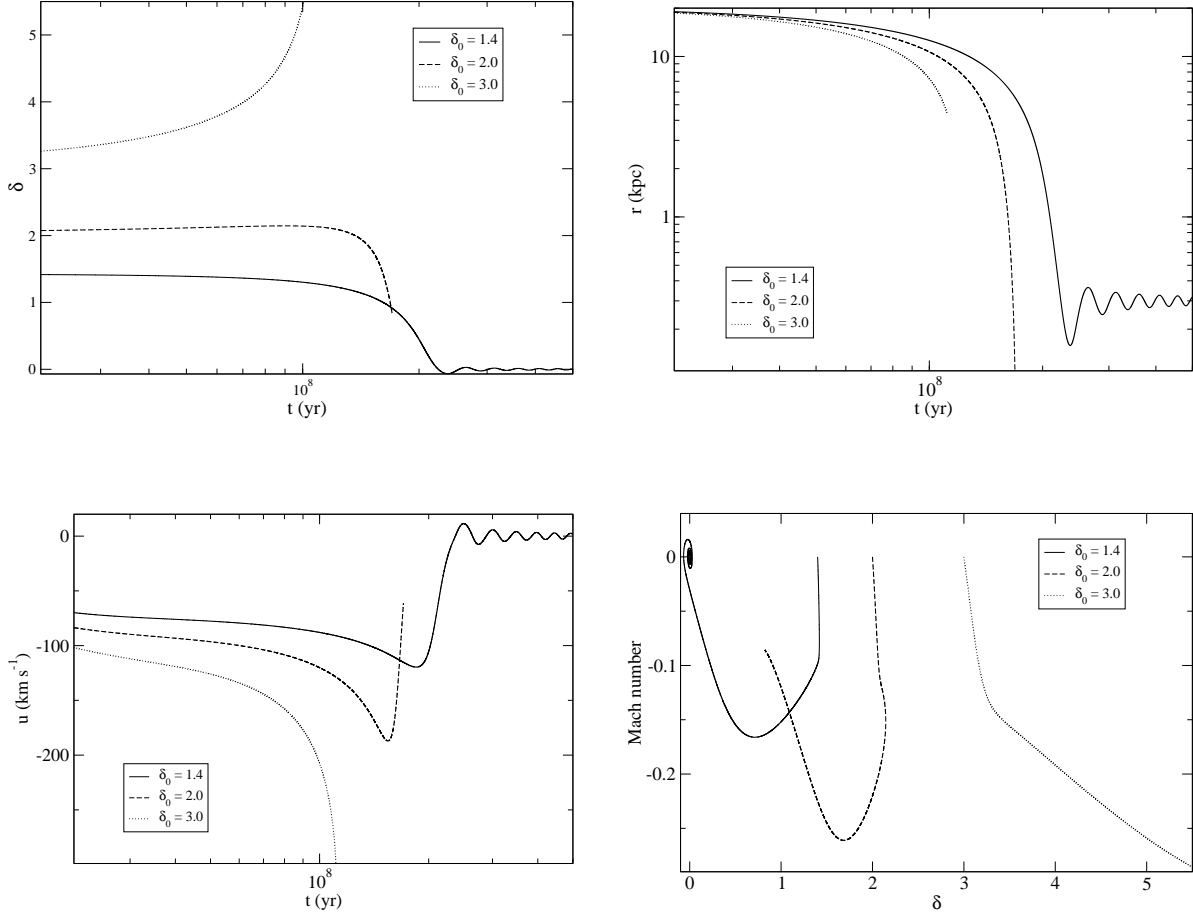


Figure 3. Tracks of a clump with an initial radius $a = 100$ pc released from $r_0 = 20$ kpc from the centre. The lines refer to different initial overdensities: $\delta_0 = 1.4$ (solid line), $\delta_0 = 2.0$ (dashed line) and $\delta_0 = 3.0$ (dotted line). Top left: overdensity vs. time; top right: radial distance vs. time; bottom left: fall velocity vs. time; bottom right: Mach number of the radial fall velocity vs. overdensity.

by Equation (7). The clump with $\delta_0 = 1.4$ is stable. Fig. 3 shows that its overdensity soon drops to zero, oscillating around zero with the Brunt–Väisälä frequency. The clump eventually reaches an equilibrium position at $r \simeq 0.3$ kpc. The trajectory of this clump in the $(\delta - \mathcal{M})$ plane (where \mathcal{M} is the ratio of the radial velocity to the local sound speed, i.e. the Mach number) winds up around the origin, which is eventually reached when the energy of the oscillations is dissipated by the drag force. The case of $\delta_0 = 2.0$ is an example of a relative instability: the overdensity decreases, but the clump is eventually accreted, since it reaches the centre of the cluster before being thermally stabilised. If the overdensity exceeds a critical value $\delta_C \simeq 2.4$ (slightly less than the estimate $\delta_C = 1.7$ calculated in Appendix A) the overdensity always increases, and the clump is eventually accreted to the centre: this is the absolute instability, shown in Fig. 3 by the case $\delta_0 = 3.0$.

The isobaric prescription for the evolution of very dense (i.e., absolutely unstable) clumps breaks down when the sound crossing time of the clumps becomes longer than its cooling time $\tau'_{\text{sound}} > \tau'_{\text{cool}}$ (Burkert & Lin 2000). For our clump with $\delta_0 = 3.0$ this happens when $\delta \simeq 32$, or $T' \simeq 0.06$ keV. The growth of the overdensity stalls after the equivalence $\tau'_{\text{cool}} \sim \tau'_{\text{sound}}$ has been reached, and from this time on the clump evolves isochorically. The subsequent evolution of the clump's temperature is difficult to estimate, but we may note that the cooling function sharply drops below $T \sim 10^4$ K (see e.g. Spitzer 1978; Sutherland & Dopita 1993), and since τ'_{cool} greatly increases, the clump is unlikely to cool much below this limit before being eventually accreted. The conclusion is that the temperature of the clumps feeding the AGN may be $T' \sim 10^4$ K, but probably not much colder.

On the other hand, a very dense clump may undergo a gravitational instability: it breaks up, decouples from the ICM and eventually freely falls to the centre. This evolution is rapid, and it may be possible that the gas of the clump encounters an atomic or molecular phase, as suggested by the presence of a large amount of molecular clouds far from the centre of clusters (Salomé et al. 2008). In this case, it is likely that the gas will cool much below 1000 K, possibly down to few tens K.

We have neglected the feedback activity of the AGN, that heats the ICM, but not the clumps. This activity increases the ICM entropy, as well as the entropy contrast between the clump and the ICM. This effect makes the clumps more unstable than found here.

The results obtained thus far are in good agreement with those presented in Paper I. The small differences are due to our different choices of the metal abundance and the cluster's temperature, density and entropy profiles.

5.1.2 *Effects of Fragmentation*

We include the description of the clumps' break up by setting the mass loss index k (Equations 20 and 21) to a positive value. Fig. 4 compares the evolution of δ for clumps with different k , but the same initial radius ($a_0 = 100$ pc) and overdensity ($\delta_0 = 1.4$); all the clumps are released from rest at the distance $r_0 = 20$ kpc from the centre. The curves in the plot refer to the mass loss indexes for the values $k = 0$, $k = 1.0$, $k = 2.0$ and $k = 4.0$. The most relevant effect of a non-vanishing k is a strong increase of the relative drag force, which suppresses the oscillations for $k \gtrsim 2$.

Fig. 5 presents the evolution of a clump with $\delta_0 = 1.4$ and mass loss index $k = 2.0$. For

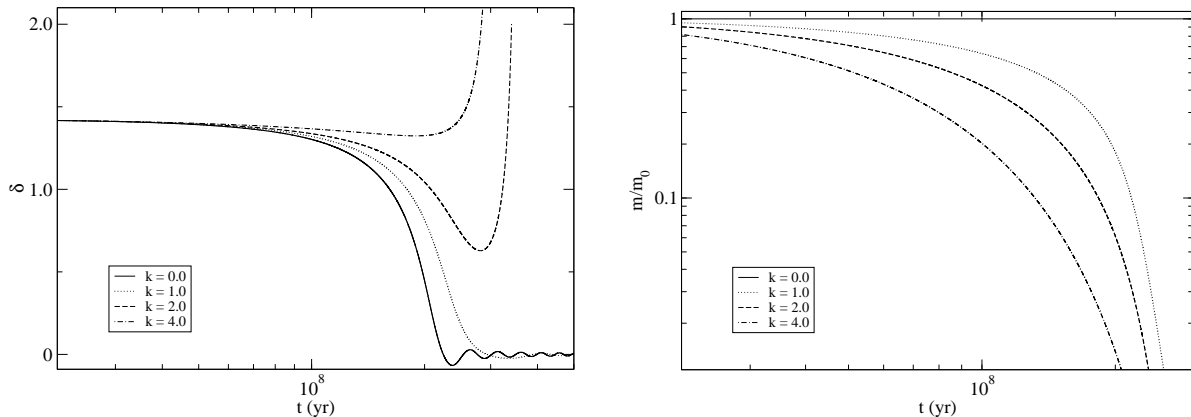


Figure 4. Evolution of the overdensity (left panel) and the mass m of a clump with respect to its initial value m_0 (right panel) for different values of the mass loss index k (eq. 20): a constant mass clump ($k = 0.0$; solid line), $k = 1.0$ (dotted line), $k = 2.0$ (dashed line) and $k = 4.0$ (large fragmentation of clump; dash-dotted line). The clump has the initial density contrast $\delta_0 = 1.4$, radius $a_0 = 100$ pc and is released with zero velocity and angular momentum from $r_0 = 20$ kpc.

comparison, we have also drawn the tracks of a clump with the same parameters, but $k = 0$. If $k = 2.0$ the drag force suppresses the oscillations and limits the fall velocity. The clump falls monotonically to the centre, and the initial decrease of its overdensity is reversed. We do not present the plots for denser clumps since the general pattern remains the same: the stronger drag force accelerates the evolution of the clump somewhat, with no other relevant qualitative effects.

Fig. 6 shows the effect of the size a of the clump on its evolution. Since the drag force behaves as $F_D \propto a^{-1}$, it effectively damps the oscillations of small clumps, whose distance from the centre then decreases monotonically. The ratio between the drag force and the force of gravity (for the same density contrast) is larger for smaller clumps. Therefore, the trend of decreasing clump's radius is like that of breaking ($k > 0$). Smaller clumps fall slower, and therefore their density contrast has time to grow, making these clumps less stable than the larger ones. On the other hand, we also expect that thermal conduction may play a role in the evolution of small clumps. As discussed in Paper I, we expect that the clumps are protected against the evaporation by magnetic fields, which suppress the thermal conduction with the ICM by a factor $\sim 10^{-3}$ (Nipoti & Binney 2004) with respect to its nominal value (as given by Braginskii 1965 or Spitzer 1962). Magnetic shielding, however, becomes inefficient for very small clumps, that will then be evaporated.

According to our phenomenological recipe (20), for moderate values of k the clumps may reach the distance $r \simeq 1$ kpc still retaining an appreciable fraction of their initial mass.

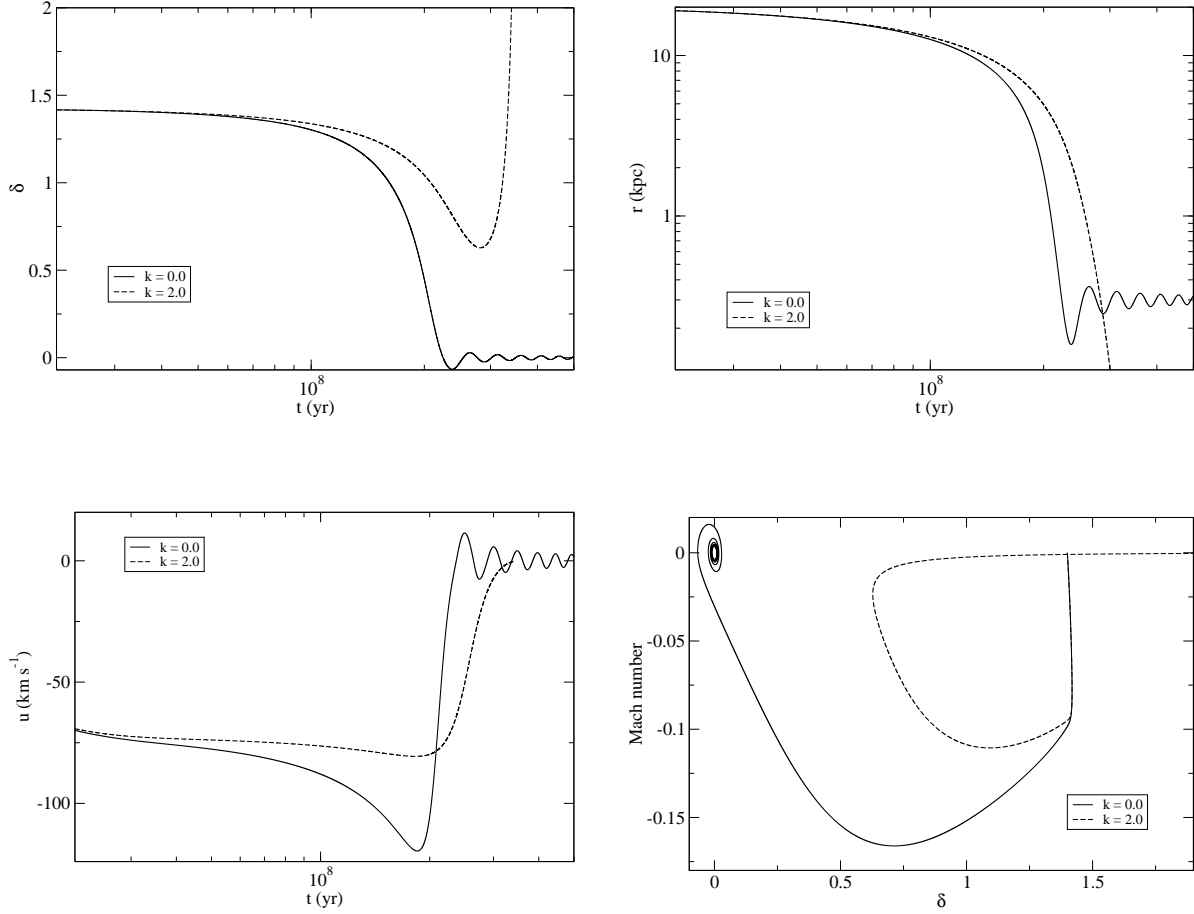


Figure 5. Dashed line: tracks of a clump with mass loss index $k = 2.0$. The initial radius and overdensity $a_0 = 100$ pc, $\delta_0 = 1.4$. The clump is released from $r_0 = 20$ kpc with zero initial velocity and angular momentum. Top left: overdensity vs. time; top right: radial distance vs. time; bottom left: fall velocity vs. time; bottom right: fall Mach number vs. overdensity. The solid lines show the evolution of a clump with the same initial parameters, but with $k = 0$. The case $k > 0$ favours the accretion process.

Although a more refined analysis is required to make reliable quantitative predictions, we are confident that this result is valid in general. At smaller radii (below $r \simeq 1$ kpc) the evolution of the clumps is different from the scenario sketched so far, as discussed later in Section 6.

5.2 Clumps with Angular Momentum

We now consider the accretion of clumps endowed with an initial orbital angular momentum. We solve the full set of equations (17), and set the initial angular momentum to

$$l_0 = \left[g_0 r_0^3 \frac{\delta_0}{1 + \delta_0} \right]^{1/2}, \quad (26)$$

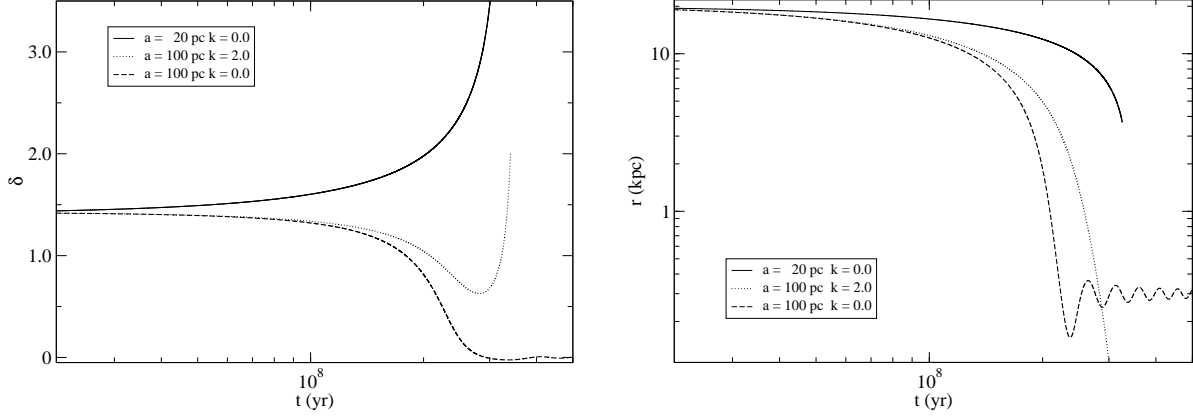


Figure 6. Evolution of overdensity (left panel) and distance from the centre (right panel) of clumps of different sizes and mass loss indices. The solid and the dashed line show the evolution of clumps with $a_0 = 20$ pc and $a_0 = 100$ pc, respectively. For both these clumps it is $k = 0$. For comparison, the dotted line shows the evolution of a clump with $k = 2.0$ and $a_0 = 100$ pc. In all cases the initial overdensity is $\delta_0 = 1.4$, and the clump is released from $r_0 = 20$ kpc with zero initial velocity and angular momentum. Smaller clumps fall slower, and therefore their density contrast has time to increase. They are less stable and more prone to the accretion process.

for which a clump with zero initial radial velocity also has zero radial acceleration (see equation 17c, where $g_0 = g(r_0)$). The clumps have the same parameters as in Section 5.1, i.e. $a_0 = 100$ pc, $r_0 = 20$ kpc and overdensities $\delta_0 = 1.4$, 2.0 and 3.0. A summary of the evolution of some relevant parameters is plotted in Fig. 7. The evolution of the overdensity is not significantly different from that found with zero angular momentum for all the clumps. As seen from the shape of the orbit (bottom left panel of Fig. 7) and from the angular momentum loss time (Fig. 8) all the clumps quickly lose their angular momentum, and their orbit becomes a straight line pointing to the centre.

The clump with $\delta_0 = 1.4$ is still stable: it reaches an equilibrium radius $r_{\text{eq}} \simeq 0.3$ kpc and oscillates around it. The denser clumps quickly become very overdense and are eventually accreted by the central black hole. The last panel of Figure 7 shows that the clumps lose their angular momentum *before* cooling. For even denser clumps this may not be the case. Fig. 9 presents the case of a clump with initial overdensity $\delta_0 = 5$. After an initial phase during which also this clump loses angular momentum, the orbit starts to wrap around the centre $(x, y) = (0, 0)$, with decreasing average distance. This clump, unlike the less dense clumps, cools down before losing its angular momentum, so its overdensity δ soon grows very large. The drag force (proportional to $(1 + \delta)^{-2/3}$) becomes very small, increasing τ_l and delaying the eventual accretion to the centre. Albeit formally correct, this solution may be unphysical for the following reasons. First, the orbital periastron of such dense clumps

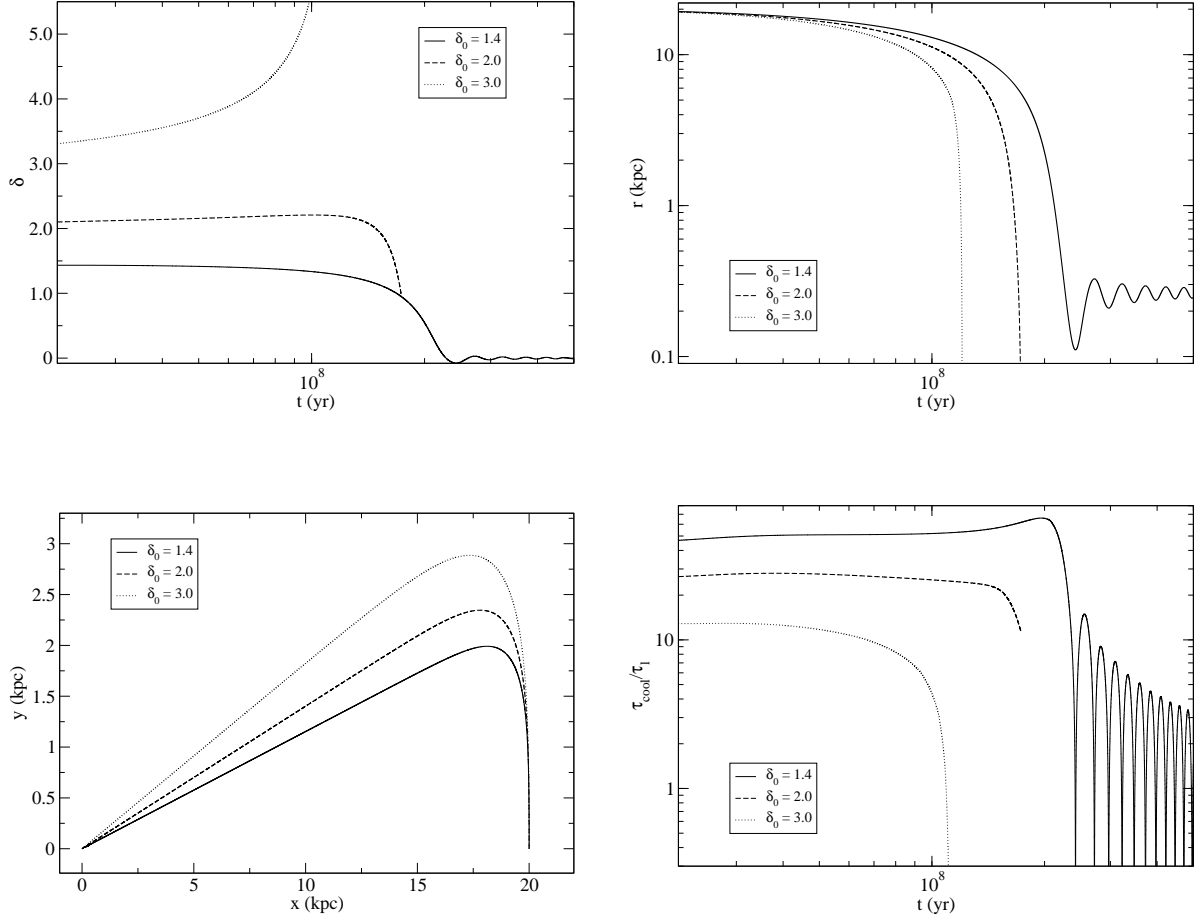


Figure 7. Tracks of a clump with initial radius $a_0 = 100$ pc released from $r_0 = 20$ kpc from the centre and having an initial angular momentum according to Equation (26). The lines refer to different initial overdensities: $\delta_0 = 1.4$ (solid line), $\delta_0 = 2.0$ (dashed line) and $\delta_0 = 3.0$ (dotted line). Top left: overdensity vs. time; top right: radial distance vs. time; bottom left: shape of the clumps' trajectories in the orbital plane (the cluster centre is at $(x, y) = (0, 0)$); bottom right: evolution of the ratio between the clump's cooling time and the angular momentum loss time.

is small (below 100 pc). As explained in Section 6, at these radii the collisions with other clumps cause the clump to efficiently lose its orbital angular momentum. This accelerates the accretion process as required by the cold feedback mechanism. Second, when the overdensity value of ~ 45 is reached (for this example, this occurs at $t \simeq 4.1 \times 10^7$ yr, when the clump is still $r \simeq 16$ kpc away from the centre), the cooling becomes isochoric rather than isobaric (Burkert & Lin 2000). The clump's compression lags behind cooling and leaves the size of the clumps larger, increasing somewhat the drag force relative to what our calculations assume at this phase.

We may summarise the main results of this section as follows: the angular momentum is quickly lost by many clumps, and their behaviour is not much different from the case with zero angular momentum presented in Paper I and in Section 5.1. This result removes

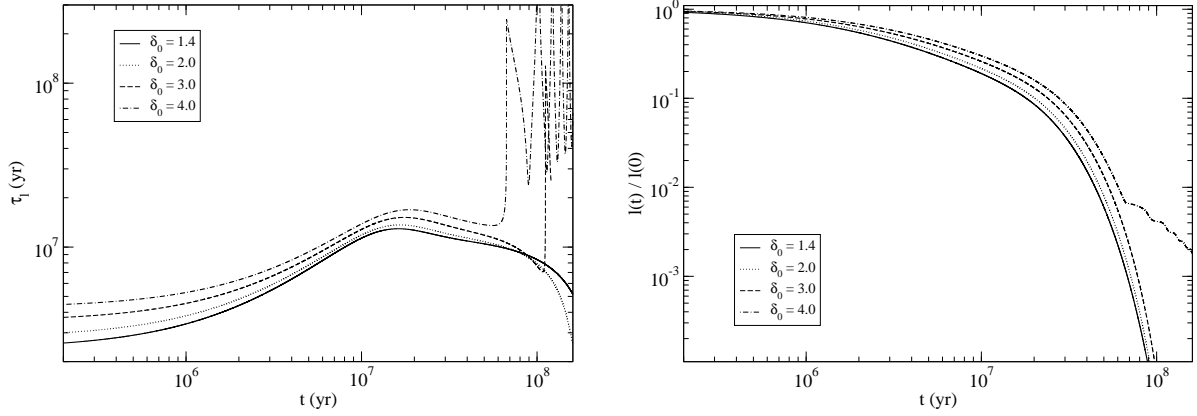


Figure 8. Evolution of the angular momentum of a clump with initial radius $a_0 = 100$ pc released from $r_0 = 20$ kpc from the centre and having initial angular momentum as in Equation (26). Left panel: the evolution of the angular momentum loss time (given by Equation 15); right panel: ratio of the angular momentum $l(t)$ with respect to its initial value $l(0)$. The lines refer to different initial overdensities: $\delta_0 = 1.4$ (solid line), $\delta_0 = 2.0$ (dotted line), $\delta_0 = 3.0$ (dashed line) and $\delta_0 = 4.0$ (dot-dashed line). The spikes in the curve $\delta_0 = 4$ are due to the modulation of the clump’s velocity on an eccentric orbit.

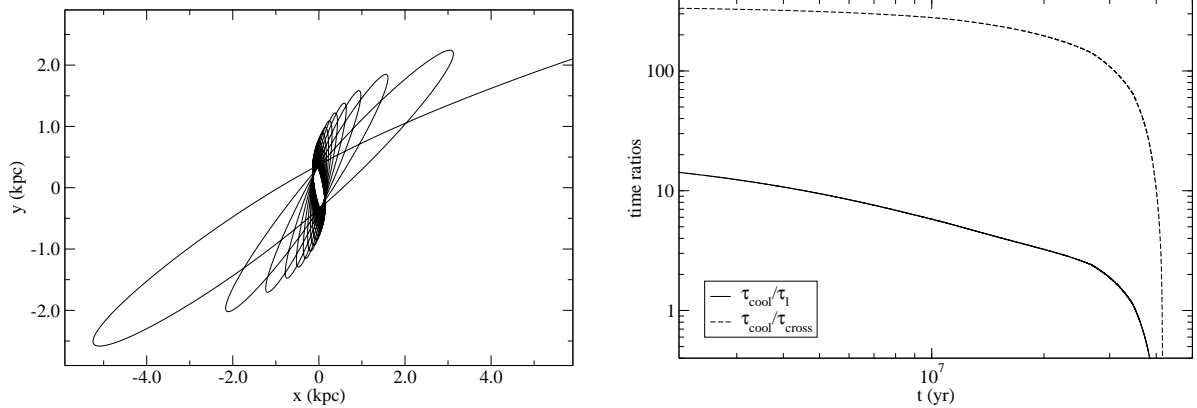


Figure 9. Evolution of a dense ($\delta_0 = 5$) clump with initial radius $a_0 = 100$ pc released from $r_0 = 20$ kpc from the centre and having initial angular momentum as in Equation (26). Left panel: the trajectory in the orbital plane. Right panel: ratio of the cooling and angular momentum loss time (solid line); ratio of the cooling and sound crossing time (dashed line).

the main obstacle that stood in the way of the cold feedback mechanism. Namely, we have shown that the response of the AGN accretion to cooling at large distances is as rapid as required.

6 COLLISIONAL BRAKING

In this section we estimate the role of collisions in the innermost region of the cluster. As the clumps fall in, they are likely to break up into smaller clumps and/or lose their spherical shape. Clumps that break up into very small pieces are likely to be evaporated by thermal

conduction (Nipoti & Binney 2004). On the other hand, clumps larger than $\sim 10 - 100$ pc (for a thermal conduction suppression factor $10^{-2} - 10^{-3}$, Fig. 3 of Nipoti & Binney 2004) will survive, and their subsequent evolution is likely dominated by mutual collisions, as explained in this section. Loss of spherical shape and fragmentation increase the cross section to volume ratio of each clump. With the higher clumps' number density near the centre, collisions between clumps are bound to occur.

Consider the clumps within a sphere S of radius r centred on the AGN. The collision time between clumps here is

$$\tau_{\text{coll}}^{-1} = \sigma v_{\text{rel}} n_c \quad (27)$$

where v_{rel} is the relative velocity of two clumps, n_c the number of clumps per unit volume within S , and σ is the collisional cross section. We take it to be the geometric cross section: $\sigma = \pi(2a)^2$, where the extra factor 2 comes from the finite size of both the target and the bullet clump. This time is to be compared with the clump's crossing time of S

$$\tau_{\text{cross}} \sim r/v_c, \quad (28)$$

where v_c is a typical clump's velocity. Random collisions are frequent if $\tau_{\text{coll}} < \tau_{\text{cross}}$, and may efficiently cause the clumps within S to lose their angular momentum. The ratio $\tau_{\text{coll}}/\tau_{\text{cross}}$ therefore estimates the efficiency of the collisional loss of angular momentum; it may be expressed in terms of the clumps' volume filling factor $\epsilon_V = 4\pi a^3 n_c/3$ as

$$\frac{\tau_{\text{coll}}}{\tau_{\text{cross}}} \simeq \frac{v_c}{v_{\text{rel}}} \frac{a}{r} \frac{1}{3\epsilon_V} \simeq \frac{a/r}{3\epsilon_V}, \quad (29)$$

where we have assumed $v_c \simeq v_{\text{rel}}$ in the last equality. For example, if $\sim 10\%$ of the clumps lose their angular momentum by collisions, then this ratio should be ~ 10 . For $r/a = 300$ (say, $r = 30$ kpc and $a = 100$ pc, or $r = 3$ kpc and $a = 10$ pc) the required efficiency demands $\epsilon_V \sim 10^{-4}$. Namely, it is sufficient that only 0.01% of the inner volume is occupied by dense clumps in the inner region. In practice, we expect ϵ_V to be larger, e.g. $10^{-3} - 10^{-2}$, depending on the mass accretion rate.

We conclude that even a small filling factor is enough to make the collisional loss of angular momentum an efficient process. The overall picture is that the drag force dominates the angular momentum loss at large radii ($r \gtrsim 1$ kpc). At smaller radii ($r \lesssim 1$ kpc) collisions dominate, causing the clumps to lose their residual orbital angular momentum.

7 CONCLUSIONS AND SUMMARY

We have studied the role of the cold clumps' angular momentum in the framework of the cold feedback model, generalizing the results of Paper I that did not include angular momentum. We first studied falling clumps with zero angular momentum. The efficiency of accretion increases (i.e., clumps are less stable) as the size of the clump decreases (for a given density contrast) and its cross section increases (for a given volume and density contrast), as evident from Figs. 4-6. The reason is that a relatively large cross section implies slower infall, such that the clump has time to increase its overdensity due to radiative cooling.

We then include angular momentum. As it is apparent from Figs. 7 and 8, at large radii the drag force is the main agent cause for clumps to lose their angular momentum, and it is efficient enough to remove the centrifugal barrier of accreted clumps. The clumps can easily reach distances of $r \lesssim 100$ pc. At this stage, the clumps may be very dense and cool ($T \lesssim 10^4$ K), and they are no more in pressure equilibrium with the surrounding ICM. As discussed in Section 6, the collisions between clumps become important, and even for small volume filling factors ($\epsilon_V \simeq 10^{-4} - 10^{-2}$) the collision time scale is comparable or shorter than the infall time. The residual orbital angular momentum is lost, and the clumps are free to accrete on the central galaxy and ultimately feed the SMBH sitting at the clusters' centre. This accretion powers the AGN and activate an efficient feedback with the ICM cooling.

In our calculations the ICM was static. However, along the jets axis there is an outflow, and clumps will not fall there freely. We expect most of the clumps to be accreted from the equatorial plane. The interaction of the jets and rising bubbles with dense clumps will be the subject of a future study. We also note that although the AGN is the main heating source, the falling clumps do release gravitational energy (Fabian 2003).

The solution of the angular momentum problem has removed the main theoretical objection to the cold feedback mechanism as a viable model for ICM heating in CF clusters. Observational support to the cold feedback mechanism (e.g., Wilman et al. 2009) stand now on a more solid ground.

ACKNOWLEDGMENTS

We are grateful to Philippe Salomé and François Combes for their valuable comments. This research was supported by the Asher Fund for Space Research at the Technion and a grant from the Israel Science Foundation.

References

- Allen S. W., Dunn R. J. H., Fabian A. C., Taylor G. B., Reynolds C. S., 2006, MNRAS, 372, 21
- Anders E., Grevesse N., 1989, *Geochim. Cosmochim. Acta*, 53, 197
- Asplund M., Grevesse N., Sauval A. J., Scott P., 2009, ARA&A, 47, 481
- Balbus S. A., Soker N., 1989, ApJ, 341, 611
- Braginskii S. I., 1965, *Reviews of Plasma Physics*, 1, 205
- Bregman J. N., Fabian A. C., Miller E. D., Irwin J. A., 2006, ApJ, 642, 746
- Burkert A., Lin D. N. C., 2000, ApJ, 537, 270
- Cavagnolo K. W., Donahue M., Voit G. M., Sun M., 2009, ApJS, 182, 12
- Ciotti L., Ostriker J. P., Proga D., 2009, ApJ, 699, 89
- Ciotti L., Ostriker J. P., Proga D., 2010, ArXiv e-prints
- Clarke T. E., Blanton E. L., Sarazin C. L., 2004, ApJ, 616, 178
- Combes F., 2008, in J. H. Knapen, T. J. Mahoney, & A. Vazdekis ed., *Pathways Through an Eclectic Universe Vol. 390 of Astronomical Society of the Pacific Conference Series, Infall and Accretion*. pp 369–381
- Edge A. C., Wilman R. J., Johnstone R. M., Crawford C. S., Fabian A. C., Allen S. W., 2002, MNRAS, 337, 49
- Edwards L. O. V., Hudson M. J., Balogh M. L., Smith R. J., 2007, MNRAS, 379, 100
- Fabian A. C., 2003, MNRAS, 344, L27
- Ghizzardi S., Molendi S., Pizzolato F., De Grandi S., 2004, ApJ, 609, 638
- Glendinning P., 1994, *Stability, Instability and Chaos*. Cambridge University Press, Cambridge, UK
- Hicks A. K., Mushotzky R., 2005, ApJ, 635, L9
- Kaiser C. R., 2003, MNRAS, 343, 1319
- Loewenstein M., 1989, MNRAS, 238, 15
- McNamara B. R., Nulsen P. E. J., 2007, ARA&A, 45, 117
- McNamara B. R., Wise M. W., Murray S. S., 2004, ApJ, 601, 173
- Nipoti C., Binney J., 2004, MNRAS, 349, 1509
- Omma H., Binney J., 2004, MNRAS, 350, L13
- Peterson J. R., Fabian A. C., 2006, *Phys. Rep.*, 427, 1
- Pizzolato F., 2007, in H. Böhringer, G. W. Pratt, A. Finoguenov, & P. Schuecker ed.,

- Heating versus Cooling in Galaxies and Clusters of Galaxies Cold Feedback in Cooling Flow Galaxy Clusters. pp 243–247
- Pizzolato F., Soker N., 2005, *ApJ*, 632, 821
- Press W. H., Teukolsky S. A., Vetterling W. T., Flannery B. P., 2007, *Numerical Recipes in C++*. The Art of Scientific Computing, third edn. Cambridge University Press, Cambridge, UK
- Rafferty D. A., McNamara B. R., Nulsen P. E. J., Wise M. W., 2006, *ApJ*, 652, 216
- Revaz Y., Combes F., Salomé P., 2008, *A&A*, 477, L33
- Russell H. R., Fabian A. C., Sanders J. S., Johnstone R. M., Blundell K. M., Brandt W. N., Crawford C. S., 2010, *MNRAS*, 402, 1561
- Salomé P., Combes F., Revaz Y., Edge A. C., Hatch N. A., Fabian A. C., Johnstone R. M., 2008, *A&A*, 484, 317
- Soker N., 2004, *MNRAS*, 350, 1015
- Soker N., 2006, *New Astronomy*, 12, 38
- Soker N., 2009, *ArXiv e-prints*
- Soker N., David L. P., 2003, *ApJ*, 589, 770
- Soker N., Sternberg A., Pizzolato F., 2009, *ArXiv e-prints*
- Soker N., White III R. E., David L. P., McNamara B. R., 2001, *ApJ*, 549, 832
- Spitzer L., 1962, *Physics of Fully Ionized Gases*, second edn. Wiley Interscience, New York
- Spitzer L., 1978, *Physical processes in the interstellar medium*. Wiley Interscience, New York
- Sutherland R. S., Dopita M. A., 1993, *ApJS*, 88, 253
- Tribble P. C., 1991, *MNRAS*, 248, 741
- Vikhlinin A., Kravtsov A., Forman W., Jones C., Markevitch M., Murray S. S., Van Speybroeck L., 2006, *ApJ*, 640, 691
- Wilman R. J., Edge A. C., Swinbank A. M., 2009, *MNRAS*, 395, 1355
- Wise M. W., McNamara B. R., Murray S. S., 2004, *ApJ*, 601, 184

APPENDIX A: EQUILIBRIUM SOLUTIONS

In this appendix we study the equilibrium solutions of equations (17) for a clump with constant mass. At equilibrium the right-hand sides of (17) vanish, which happens if $v = 0$, $l = 0$, $\delta = 0$; r and ϕ are both constant. It is clear that since $\delta = 0$ the clump is indistinguishable from the ICM, so this equilibrium solution describes a clump reabsorbed by the ICM. It is worth noting that such an equilibrium solution is allowed only if the cooling of the ICM is accounted for, which was not in Paper I.

The linearised system (17) reads

$$\frac{dr}{dt} = u \quad (\text{A1a})$$

$$\frac{du}{dt} = -g \delta \quad (\text{A1b})$$

$$\frac{d\delta}{dt} = \frac{3}{5} u \frac{d \ln K}{dr} + \frac{\omega'}{\tau_{\text{cool}}} \delta, \quad (\text{A1c})$$

where

$$\omega' = \left. \frac{\partial \omega}{\partial \delta} \right|_{\delta=0} = 2 - \frac{d \ln \Lambda}{d \ln T} \quad (\text{A2})$$

and

$$\tau_{\text{cool}}^{-1} = \frac{2}{5} \frac{\mu_H n_e \Lambda(T)}{k_B T} \quad (\text{A3})$$

is the inverse of the ICM cooling time.

The linearised system admits solutions $\delta \propto u \propto e^{\lambda t}$ if λ is the root of the characteristic equation

$$\lambda \left(\lambda^2 - \frac{\omega'}{\tau_{\text{cool}}} \lambda + \omega_{\text{BV}}^2 \right) = 0, \quad (\text{A4a})$$

where the (squared) Brunt–Väisälä frequency

$$\omega_{\text{BV}}^2 = -\frac{3}{5} \mathbf{g} \cdot \nabla \ln K = \frac{3}{5} \frac{g}{r} \frac{d \ln K}{d \ln r} \quad (\text{A4b})$$

is positive in a convectively stable cluster. For typical parameters $\omega_{\text{BV}} \gg \tau_{\text{cool}}^{-1}$, so the eigenvalues are

$$\lambda = 0 \quad \lambda \simeq \omega'/2 \tau_{\text{cool}} \pm i \omega_{\text{BV}}. \quad (\text{A5})$$

One of the eigenvalues is zero, so the equilibrium is non-hyperbolic and a simple linear analysis does not suffice to characterise the global stability of the system (see e.g. [Glendinning 1994](#)). The perturbations oscillate around the equilibrium position with the Brunt–Väisälä frequency. If ω' (defined by Equation A2) is positive, the perturbations' amplitude grows on a cooling time. The reason of this (overstable) growth is easily understood:

after the clump has completed an oscillation, its density has grown a little on account of the radiative losses, which causes the amplitude of its next oscillation to be larger. The overstability criterion $\omega' > 0$ was already found and discussed by [Balbus & Soker \(1989\)](#): in particular see their equation (2.1), with $\mathcal{L} = n^2 \Lambda(T)$. The oscillations' amplitude of an overstable clump will soon grow so large that it is not possible to disregard the non-linear terms of the equation, invalidating this simple linear analysis.

The global behaviour of the system may be studied in the “reduced” set of equations made by the velocity and overdensity equations only. In this system r is merely a constant parameter. With a suitable scaling of the variables, the reduced system reads

$$\frac{1}{1+\delta} \frac{d\delta}{dt} = u + \xi \omega(\delta, T) \quad (\text{A6a})$$

$$(1+\delta) \frac{du}{dt} = -\eta \left(\frac{1+\delta}{1+\delta_0} \right)^{1/3} |u|u - \delta, \quad (\text{A6b})$$

where

$$\eta = \frac{3}{8} C_D \frac{g}{a_0 \omega_{\text{BV}}^2} \quad \xi = (\omega_{\text{BV}} \tau_{\text{cool}})^{-1}. \quad (\text{A6c})$$

This system admits the trivial solution $\delta = u = 0$: this is the only proper equilibrium solution of the total system, since the velocity must vanish there. The non-trivial equilibrium solutions are

$$|u|u = -\frac{\delta}{\eta} \left(\frac{1+\delta_0}{1+\delta} \right)^{1/3} \quad u = -\xi \omega(\delta, T). \quad (\text{A7})$$

The first equation gives the negative (inwards) velocity

$$u_t = - \left[\frac{\delta}{\eta} \left(\frac{1+\delta_0}{1+\delta} \right)^{1/3} \right]^{1/2}. \quad (\text{A8})$$

This is the “terminal” velocity of a clump, resulting from the equilibrium between the gravitational pull and the drag force. The overdensity corresponding to the velocity u_t is implicitly defined by the equation

$$\delta_t \left(\frac{1+\delta_0}{1+\delta_t} \right)^{1/3} = \chi \omega_t^2, \quad (\text{A9})$$

where $\chi = \eta \xi^2$ and $\omega_t \equiv \omega(\delta_t, T)$. This formula will be useful in a moment to derive a simple stability criterion for the thermal stability of a clump.

The study of the eigenvalues of the jacobian matrix to assess the stability of the equilibrium points $\mathcal{O} = (0, 0)$ and $\mathcal{A} = (\delta_t, u_t)$ is not particularly illuminating. It is more convenient to plot (Fig. [A1](#)) the directions of the vector fields $d\delta/dt$ and du/dt given by [\(A6\)](#). The lines defined by the equalities $d\delta/dt = 0$ (dashed line) and $du/dt = 0$ (solid line) divide the plane $(\delta - u)$ into five regions, labelled I, II, III, IV, V. A point starting from the upper

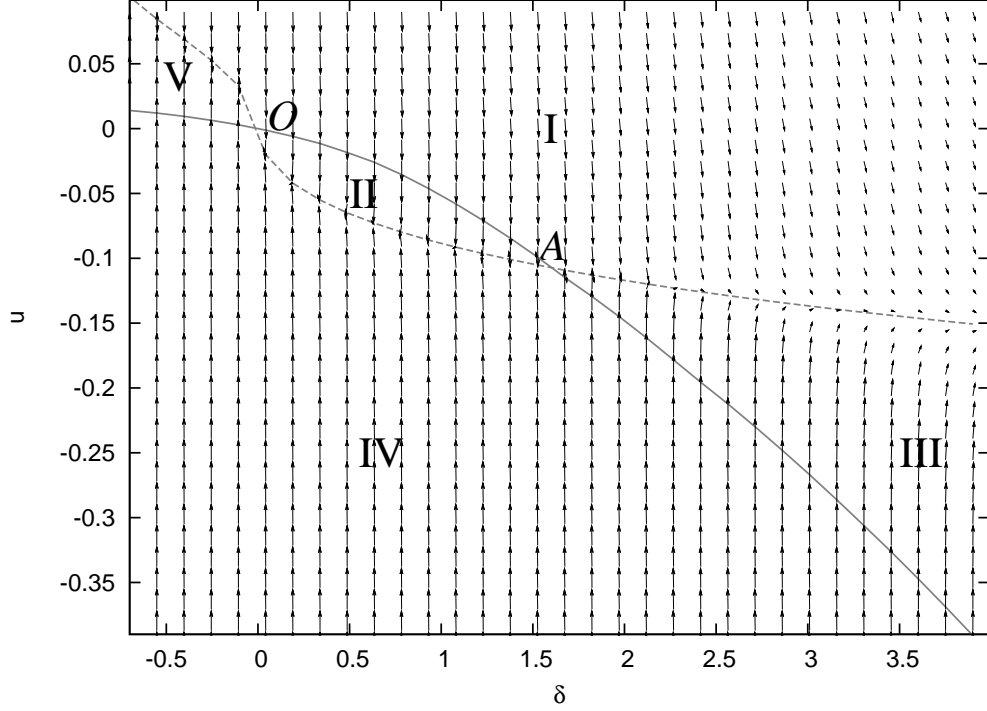


Figure A1. Vector fields defined by the reduced equation system (A6). The dimensionless parameters (defined in Appendix A) are $\eta = 1.27 \times 10^2$, $\xi = 1.64 \times 10^{-2}$ and $\chi = 3.42 \times 10^{-2}$. They correspond to a clump of radius $a_0 = 100$ pc released from rest at the radius $r_0 = 20$ kpc in a cluster like Virgo. The points for which $d\delta/dt = 0$ lie on the solid line, the points for which $du/dt = 0$ lie on the dashed line.

right of region I drifts to the lower right of the plane, i.e. its overdensity increases without limits, and its velocity approaches the terminal velocity (A8). If the initial position is on the left of region I, the trajectory crosses vertically the solid line, moves leftwards to region II, and crosses horizontally the dashed line, moving to region IV. The trajectory coasts the dashed line, moving to region V and finally to region I again. The overdensity is now smaller than the initial one, and this trajectory winds up around the point \mathcal{O} , which is stable. This behaviour shows the existence of a critical initial overdensity δ_C . If $\delta_0 > \delta_C$ the clump is (absolutely) unstable: its overdensity grows more and more, and it is eventually accreted on the cluster centre.

We now derive simple formula for the critical density δ_C of a clump released from rest. Consider the trajectory of a clump in the $(\delta - u)$ plane. The starting point of a clump released with zero velocity is $\mathcal{S} = (\delta_0, 0)$. In a neighbourhood of \mathcal{S} the trajectory may be approximated by the straight line

$$u = u'(\delta - \delta_0), \quad (\text{A10})$$

where

$$u' = -\frac{\delta_0}{(1 + \delta_0)^2 \xi \omega_0} \quad (\text{A11})$$

is the derivative $du/d\delta$ evaluated at \mathcal{S} , and $\omega_0 \equiv \omega(\delta_0, T)$. The line joining \mathcal{S} and \mathcal{A} has (negative) angular coefficient

$$m = \frac{u_t}{\delta_t - \delta_0}, \quad (\text{A12})$$

where $u_t = -\xi \omega_t$, according to the second equation A7. If $u' = m$ the trajectory originating in \mathcal{S} hits the point \mathcal{A} : the value of δ_0 for which this occurs corresponds to the critical overdensity δ_C ; if $|u'| < |m|$ the trajectory entirely lies in the region I of the $(\delta - u)$ plane (Fig. A1), and if $|u'| > |m|$ the clump moves to region II, and its overdensity decreases. The equation $u' = m$ reads

$$\frac{\delta_C}{(1 + \delta_C)^2 \xi \omega_C} = \xi \frac{\omega_t}{\delta_t - \delta_C}. \quad (\text{A13})$$

Equations (A9) (with $\delta_0 = \delta_C$) and (A13) provide a closed system for δ_C and δ_t . This system is quite complex, but it may be simplified under the assumption $\xi \ll 1$, which is true for typical parameters. We may therefore expand

$$\delta_C = \delta_t + \xi \delta_C^{(1)} + \xi^2 \delta_C^{(2)} + o(\xi)^2 \quad (\text{A14})$$

To zero order in ξ Equation (A13) simply gives $\delta_C = \delta_t$, and Equation (A9) becomes $\delta_t = \chi \omega_t^2$. This equation in δ_t may be solved numerically, with the temperature T entering as a parameter. Plugging the expansion (A14) into Equation (A13) and comparing the coefficients of the powers of ξ we find $\delta_C^{(1)} = 0$ and $\delta_C^{(2)} = \omega_t^2 (1 + \delta_t)^2 / \delta_t$, to give

$$\delta_C = \delta_t + \xi^2 \frac{\omega_t^2 (1 + \delta_t)^2}{\delta_t} + o(\xi)^2. \quad (\text{A15})$$

Since $\xi \simeq 10^{-2} \ll 1$, the zero-order approximation is usually satisfactory. In this case the value $\delta_C \simeq \delta_t$ only depends on the dimensionless parameter χ ; a couple of examples are shown in Fig. A2 for different temperatures.

Fig. A3 shows the radial profile of δ_C —as calculated from the second-order formula (A15)— for some values of the clumps' initial radius a_0 . The radial temperature, density and entropy profiles are those of the Virgo cluster.

A final warning about this stability analysis is in order. In the present analysis we have neglected the motion of the clump through the cluster: the radius entered only implicitly into the coefficients η and ξ , treated as constants. If the radial motion of the clump is considered, the situation is slightly more involved. First, the clump slightly drifts inwards, and its evolution occurs at a smaller distance to the centre, where δ_C is larger (if $r \gtrsim 0.2$ kpc,

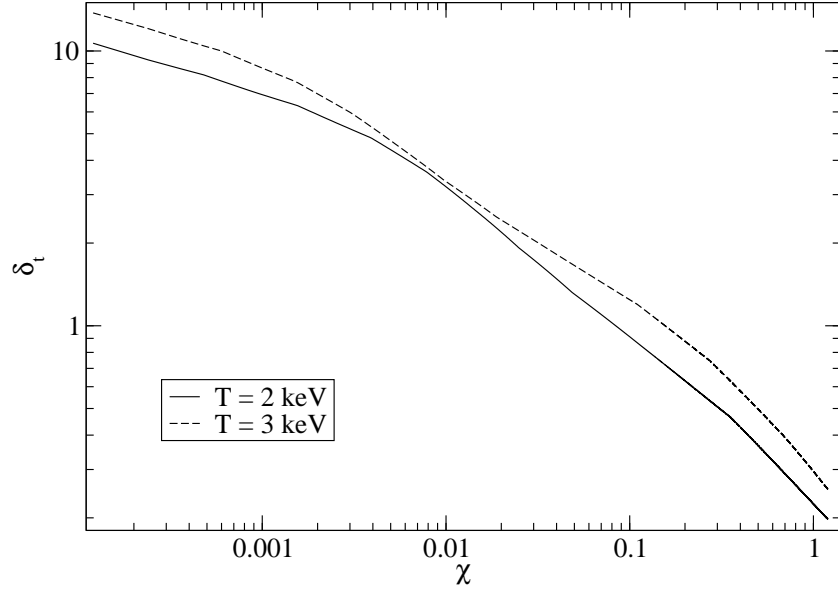


Figure A2. Critical overdensity δ_t , above which constant mass clumps are thermally unstable. δ_t is plotted against the dimensionless stability parameter χ defined by Equation (A9). The function ω (defined by Equation 13) has been evaluated at $T = 2.0$ keV (solid line) and $T = 3.0$ keV (dashed line).

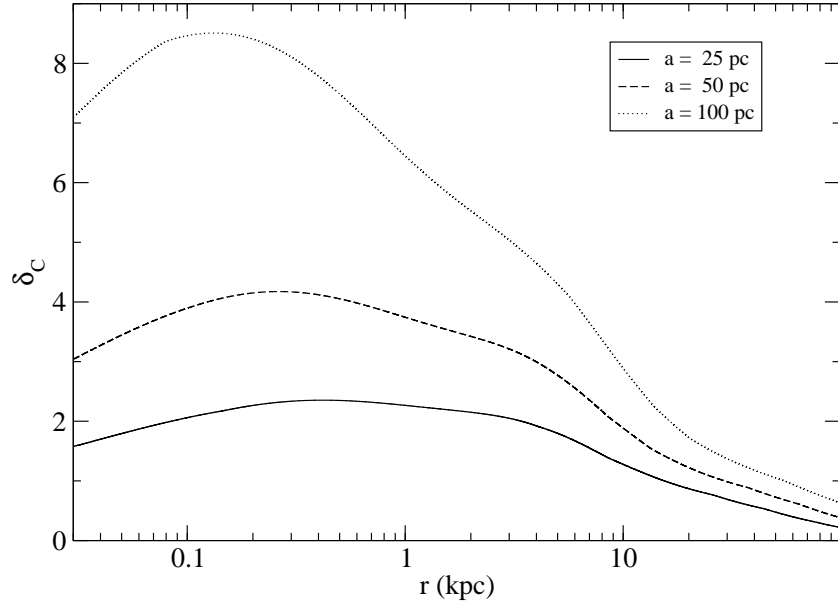


Figure A3. Critical overdensity δ_C , above which constant mass clumps are thermally unstable as a function of the distance from the centre, for Virgo. The curves refer to different initial radii of the clumps: $a_0 = 25$ pc (solid line); $a_0 = 50$ pc (dashed line) and $a_0 = 100$ pc (dotted line). Clumps with $\delta > \delta_C$ are accreted, the other are thermally stabilised at $r > 0$.

Fig. A3). The value of δ_C found with the analysis of the reduced system (A6) is therefore slightly underestimated. Second, even a clump with $\delta < \delta_C$ may be accreted to the centre: we term this behaviour as “relative instability”. If δ_0 is not much smaller than δ_C , the clump’s overdensity decreases, but the clump may nevertheless reach the centre before the equilibrium value $\delta = 0$ is attained. The value δ_C calculated here may only distinguish between the “relative instability” (for which $\dot{\delta} < 0$, with *possible* eventual accretion) and the “absolute instability”, for which $\dot{\delta} > 0$ all the way.

This paper has been typeset from a T_EX/ L^AT_EX file prepared by the author.